Applied Physics Letters

Electron-lattice coupling in bound-to-continuum THz quantum-cascade lasers

Cite as: Appl. Phys. Lett. **88**, 241109 (2006); https://doi.org/10.1063/1.2211301
Submitted: 12 January 2006 . Accepted: 04 May 2006 . Published Online: 14 June 2006

Miriam S. Vitiello, Gaetano Scamarcio, Vincenzo Spagnolo, Tonia Losco, Richard P. Green, Alessandro Tredicucci, Harvey E. Beere, and David A. Ritchie

AIP Publishing

Electron-lattice coupling in bound-to-continuum THz quantum-cascade lasers

Miriam S. Vitiello[a] and Gaetano Scamarcio
CNR-INFM Regional Laboratory LIT3 and Dipartimento Interateneo di Fisica "M. Merlin," Università degli Studi di Bari, Via Amendola 173, 70126 Bari, Italy

Vincenzo Spagnolo
CNR-INFM Regional Laboratory LIT3 and Dipartimento Interateneo di Fisica "M. Merlin," Politecnico di Bari, Via Amendola 173, 70126 Bari, Italy

Tonia Losco, Richard P. Green, and Alessandro Tredicucci
NEST-CNR-INFM and Scuola Normale Superiore, Piazza dei Cavalieri 7, 56126 Pisa, Italy

Harvey E. Beere and David A. Ritchie
Cavendish Laboratory, University of Cambridge, Madingley Road, Cambridge CB3 0HE, United Kingdom

(Received 12 January 2006; accepted 4 May 2006; published online 14 June 2006)

We measured the thermal resistance ($R=20.1$ K/W) and the electrical power dependence of the electronic temperature ($R_e=27.0$ K/W) of THz quantum-cascade lasers (QCLs) with bound-to-continuum active region scheme in the lattice temperature range of 30–100 K. This information, obtained from the analysis of microprobe photoluminescence spectra for QCLs operating at 2.5 THz, gives an electron-lattice energy relaxation rate (0.1 ps^{-1}) ~50 times lower than THz QCLs with resonant-phonon active region scheme. © *2006 American Institute of Physics*. [DOI: 10.1063/1.2211301]

The quantum-cascade laser (QCL) is one of the most promising compact sources for the generation of far-infrared coherent radiation.[1] Electron energy relaxation processes such as e-e, electron-longitudinal optical (LO) phonons, impurity, and interface roughness scattering jointly with free-electron absorption processes affect the operating efficiency of QCLs, leading to the establishment of a nonequilibrium electronic distribution that strongly influences the device high temperature operation. In THz QCLs the intersubband energy spacing is typically smaller than the LO-phonon energy. Therefore the LO-phonon emission is drastically reduced, whereas the e-e scattering becomes relevant. The optimization of the active region design based on the bound-to-continuum[2,3] (BTC) or the resonant-phonon[4] schemes allowed the achievement of low threshold current densities[3,5] or high operating temperatures in the range of 137–160 K (Ref. 4) in the spectral range of 2–4.8 THz.

Recently, we have studied the hot-electron distribution in resonant-phonon THz QCLs.[6] We found that the performance of this class of devices is strongly influenced by the high electronic temperature of the excited laser level and that the electron-lattice energy relaxation rate is comparable with that of mid-IR QCLs.[7] In this work, we focus on the BTC scheme.[3] A miniband is used for the depopulation of the lower radiative state via e-e scattering. The upper radiative state is designed to fall in the first minigap in order to have a diagonal laser transition to enhance carrier injection and decrease nonradiative scattering into the lower miniband.

In this letter we report on the simultaneous determination of the electronic (T_e) and lattice (T_L) temperatures both below and above the laser threshold as a function of the electrical power (P) in high-performance QCLs, based on the BTC scheme and operating at 2.5 THz. The calculated conduction and valence band structures are shown in Fig 1. A detailed description of the device structure is reported in Ref. 3. Our approach is based on the analysis of band-to-band photoluminescence (PL) spectra measured in devices operating in continuous mode. PL spectra were obtained by focusing the 647 nm line of a Kr^+ laser onto the laser facet down to a spot size of ≈2.5 μm, using an optical power density as low as ~245 W/cm^2. The laser excitation mostly provides the valence band holes needed to probe the electronic population via band-to-band radiative recombination. The detailed description of the PL apparatus is reported in

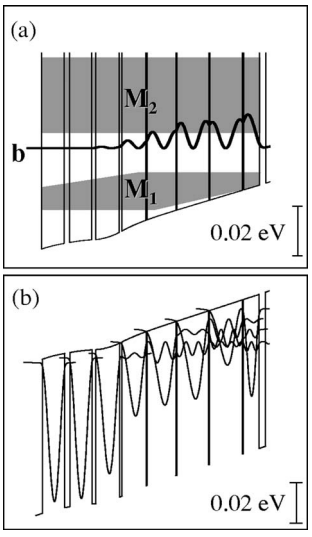

FIG. 1. Conduction (a) and valence (b) band structures of 1period of the investigated sample calculated using a self-consistent Schrödinger-Poisson solver at 28.2 mV per stage. A 66% conduction band offset is used. The thicknesses in nm of the layers are (from right to left, starting at the injection barrier) 3.9/9.6/0.6/19.9/0.6/19.4/0.6/17.5/0.6/14.7/1.5/14.4/2.4/13.4/3.2/13.7. A 10 nm thick portion of the underlined GaAs well is doped to $n=2.5\times10^{16}$ cm^{-3}. The shaded area M_1 (M_2) represents the lowest energy (a higher energy) miniband. The wave function square modulus of the excited laser state (bound level) is labeled as b.

[a]Electronic mail: vitiello@fisica.uniba.it

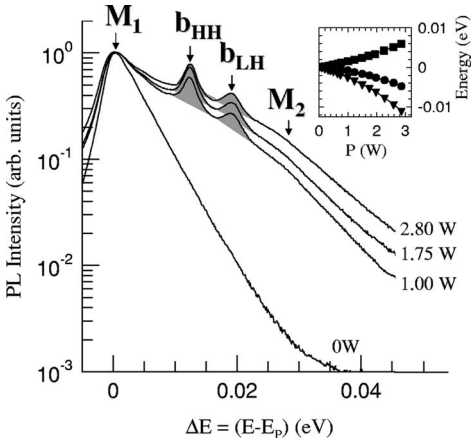

FIG. 2. Representative photoluminescence spectra measured at different electrical powers (P), each plotted as a function of the energy difference ΔE with respect to the corresponding main peak energy E_P. The heat sink temperature is 35 K. The arrows labeled with M_j mark the energies of the transitions between levels in the conduction minibands (M_j) and valence subbands [see Figs. 1(a) and 1(b)]. The arrows marked with b_{HH} and b_{LH} indicate the heavy-hole and light-hole exciton peaks. Inset: Measured shift ΔE_P of the main peak energy (●), calculated variation of conduction and valence subbands confinement factors $\Delta(E_C+E_V)$ (■), and band gap thermal shift ΔE_g (▼) plotted as a function of P. The lines are guides for the eye.

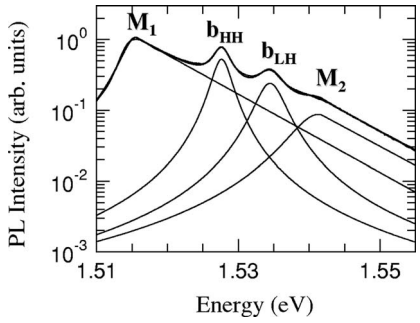

FIG. 3. Dashed line: Photoluminescence spectrum at $P=2$ W. Solid line: Calculated PL components peaked at the theoretical energies of relevant band to band transitions. The low energy side of the curves labeled as M_1 and M_2 is a Lorentzian. The high energy side is an exponential decay function $\propto\exp[E/k_BT_e^j]$. The curves labeled b_{HH} and b_{LH} are Lorentzians. The experimental data have been fitted leaving $T_e^{M_1}$, $T_e^{M_2}$ the band intensities and the linewidth of the HH and LH exciton peak as fitting parameters.

Ref. 8. We use the facet temperature as a close estimate of the internal one due to the absence of nonradiative surface electron-hole recombination processes in unipolar devices. Experimental investigations based on an interferometric thermal mapping technique[9] showed that the temperature does not change along the waveguide.[10,11]

Figure 2 shows a set of representative PL spectra collected at different P values. The peak energy (E_P) of the main PL band varies with P due to the combined effects of Joule heating and quantum confinement. Each spectrum is plotted as a function of the energy difference ΔE with respect to the corresponding E_P value. At zero current, the PL spectrum shows a single band associated with band-to-band transitions between levels in the injector miniband M_1, where the vast majority of electrons sit and valence subbands. When electrons are tunnel injected into the excited laser level b, additional features appear on the high energy tail of the main PL band. The two peaks at $\Delta E=0.012$ eV and $\Delta E=0.018$ eV are ascribed to the heavy-hole (b_{HH}) and light-hole (b_{LH}) excitons arising from level b. This assignment is supported by the following facts: (i) energy level calculations show that the b_{HH} and b_{LH} peaks can be associated with level b only, whereas assignments involving the active region minibands M_1 and M_2 are excluded; (ii) the energy separation (b_{HH}-$b_{\mathrm{LH}}\sim 6$ meV) is coincident with the HH-LH splitting of excitons in large (17–18 nm) GaAs quantum wells;[12] and (iii) the line shape is Lorentzian[13] with a small linewidth (1.3–1.6 meV),[14] as shown in Fig. 3 and discussed later.

The observation of excitons associated with ground state subbands in PL spectra is a well studied subject. Experiments show that the threshold concentration at which the collapse of excitons due to the charge induced screening of the Coulomb potential takes place is sample dependent and reaches the value $n_c\sim 10^{10}$ cm^{-2} in quantum structures grown under the same experimental conditions of the investigated devices.[15] In our structure excitons associated with the miniband M_1 cannot be observed because the electron sheet density $(3.5\times 10^{10}\ \mathrm{cm}^{-2})>n_c$ in the leftmost four quantum wells of Fig. 1(a). The condition for the observation of excitons associated with excited states is much less known. On the other hand, the wave function of level b mainly extends in an 85 nm thick spatial region [four rightmost quantum wells in Fig. 1(a)] characterized by a negligible static electronic density and the level of carrier injection on subband b is at least one order of magnitude lower than that of the injector subbands. The Debye screening length $\lambda_D=9-15$ nm in the investigated lattice temperature range. Hence, stable excitons associated with level b can exist in our samples.[16] Previous PL experiments on resonant-phonon THz QCLs did not show evidence of excitonic structures.[6] This is due to the much smaller spatial extension of the upper laser level wave function ($\sim$17 nm), comparable with λ_D (15–22 nm). Finally, we ascribe the high energy band at $\Delta E\sim 0.028$ eV in Fig. 2 to transitions involving conduction subbands confined in the miniband (M_2) that becomes progressively populated with the applied electric field.

The redshift of the main PL peak as a function of P can be used to extract the device local lattice temperature, provided that the calculated field induced shift of the confinement energies is properly considered. The following relation holds: $\Delta E_g=\Delta E_P-\Delta(E_C+E_V)$, where E_C and E_V are the ground state conduction and valence band confinement energies, respectively. $\Delta \mathrm{E}_g$ is the temperature induced shift of the energy gap. In the inset of Fig. 2 the measured value of $\Delta \mathrm{E}_p$, the calculated values of $\Delta(E_C+E_V)$, and the resulting $\Delta \mathrm{E}_g$ are plotted as a function of P. Comparison of $\Delta \mathrm{E}_g$ with a calibration curve, collected by probing the device at zero current while varying the heat sink temperature, gives T_L

The electronic temperatures were extracted from the line shape analysis of PL spectra. In the case of band-to-band transitions, the fitting function was obtained by joining a Lorentzian on the low energy side with an exponential decay $\propto\exp[-E/k_BT_e^{M_j}]$ on the high energy side.[6] Due to the close energy spacing of the conduction subbands, we assumed a common electronic temperatur $T_e^{M_j}$ within each miniband. For excitonic peaks, Lorentzian line shape functions, characteristic of exciton PL bands in the presence of homogeneous broadenings and weak exciton-phonon coupling,[13] have been used. Figure 3 illustrates the application of this method to the PL spectrum collected at $P=2$ W.

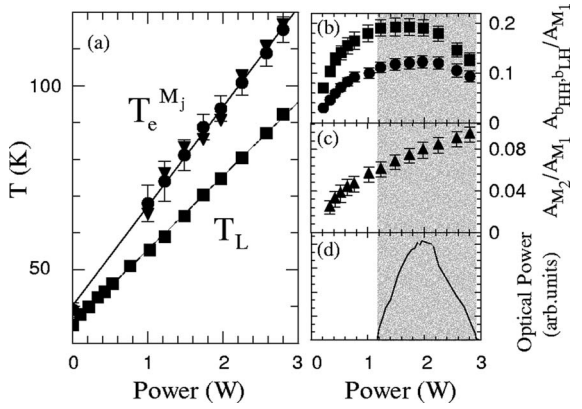

FIG. 4. Mean lattice temperature T_L (■) and miniband electronic temperatures $T_e^{M_1}$ (●), $T_e^{M_2}$ (▼) in the active region of the investigated device measured as a function of the electrical power (P) at the heat sink temperature of $T_H=35$ K. The lines are linear fits to the data. (b) Ratios between the areas of the PL bands b_{HH}, M_1 (■) and b_{LH}, M_1 (●) plotted as a function of P. (c) Ratios between the areas of the PL bands M_2 and M_1 plotted as a function of P. (d) Peak optical power plotted as a function of P measured at $T_H=35$ K. The shaded area marks the lasing region.

The electronic and lattice temperatures $T_e^{M_j}$ and T_L are plotted in Fig. 4(a) as a function of P. The fitting procedure to extract $T_e^{M_1}$ and $T_e^{M_2}$ was restricted to the range $P \geqslant 1$ W, where tunnel injection into the upper laser level becomes efficient. The electronic temperatures of subbands belonging to the minibands M_1 and M_2 are coincident within ~3 K and increase linearly with P with a slope $R_e=27.0$ K/W, larger than the thermal resistance $R=dT_L/dP=20.1$ K/W. The existence of a common T_e value in the active region subbands demonstrates that the vast majority of electrons share the same electronic temperature. Due to the excitonic nature of the PL peaks arising from electrons that populate the upper laser level b we cannot extract the electronic temperature of this level. However, the line shape analysis allows to estimate the electronic population of level b with respect to that of the active region injector miniband.

Figure 4(b) shows the ratios $A_{b_{HH}}/A_{M_1}$ and $A_{b_{LH}}/A_{M_1}$ between the areas of the PL bands b_{HH}, M_1 and b_{LH}, M_1 plotted as a function of P. For comparison, the ratio between the areas of the bands M_2 and M_1 is also plotted in Fig. 4(c). The ratio A_{M_2}/A_{M_1} increases in the investigated P range. Both ratios $A_{b_{HH}}/A_{M_1}$ and $A_{b_{LH}}/A_{M_1}$ increase up to the laser threshold (1.20 W), remain nearly constant from the threshold to the rolloff (2.20 W), likely reflecting the clamping of the optical gain, and decrease at $P>2.20$ W due to the reduction of the injection efficiency into level b. The latter effect and the increased current leakage into the miniband M_2 lead to the ceasing of the laser action at $P \approx 2.95$ W. In particular, the leakage channel represents key limiting factors for the device high temperature operation ($T_{max}=50$ K).

From the measured R_e and R values we calculated a difference $(R_e-R)=6.9$ K/W, significantly higher than that measured in the case of resonant-phonon QCLs.[7] This value is determined by the energy exchange rates between electrons, optical phonon, and acoustic phonon subsystems and demonstrates that the electron-phonon interaction is not strong enough to efficiently dissipate the electron extra energy via optical-phonon emission. The calculated electron-lattice energy relaxation rate[6,17,18] $\tau_E^{-1}=0.1$ ps^{-1} can be compared with that, significantly higher, measured in the case of resonant-phonon THz QCLs ($\tau_E^{-1}=4.9$ ps^{-1}). The huge difference can be explained by considering that in BTC devices due to the low intersubband spacing (<0.036 eV) the e-e scattering becomes the dominant channel for carrier thermalization, while cooling of the electronic ensemble is assured by e-LO-phonon scattering only for those electrons that acquire sufficient energy by e-e or e-interface roughness scattering. Most of the electrons dissipate their excess energy via the less efficient acoustic phonon-assisted transitions. This is very different from the case of mid-IR or resonant-phonon THz QCLs that use LO-phonon assisted transitions as the main depletion mechanism, thus allowing an efficient cooling of the electronic ensemble. As a consequence, in the case of BTC structures, the electron energy relaxation is less efficient. This is a relevant aspect of temperature performance degradation in BTC THz QCLs and should be considered for the design of optimized quantum structures, aiming at better temperature performance. Possible solutions are (i) the insertion of a phonon stage,[19,20] by adding a wide well, between the active region and the injector to assure a more efficient electronic cooling and (ii) the design of more diagonal optical transitions to increase the upper laser level lifetime and the injection efficiency, thus reducing the leakage channels.

This work was partially supported by MIUR (DD 1105/2002) and by the IST project Teranova, the PASR project Terasec, and the Marie Curie RTN Poise. C. Pflügl, A. Wacker, M. Dabbicco, and S. Luin are gratefully acknowledged for helpful discussions.

[1] R. Köhler, A. Tredicucci, F. Beltram, H. E. Beere, E. H. Linfield, A. G. Davies, D. A. Ritche, R. C. Iotti, and F. Rossi, Nature (London) **417**, 156 (2002).
[2] L. Ajili, G. Scalari, J. Faist, H. E. Beere, E. H. Linfield, A. Ritchie, and A. G. Davies, Appl. Phys. Lett. **85**, 3986 (2004).
[3] L. Mahler, A. Tredicucci, R. Kohler, F. Beltram, H. E. Beere, E. H. Linfield, and D. A. Ritchie, Appl. Phys. Lett. **87**, 181101 (2005).
[4] B. S. Williams, S. Kumar, Q. Hu, and J. Reno, Opt. Express **13**, 3331 (2005).
[5] C. Worrall, J. Alton, M. Houghton, S. Barbieri, H. E. Beere, D. A. Ritchie, and C. Sirtori, Opt. Express **14**, 171 (2006).
[6] M. S. Vitiello, G. Scamarcio, V. Spagnolo, B. S. Williams, S. Kumar, Q. Hu, and J. L. Reno, Appl. Phys. Lett. **86**, 11115 (2005).
[7] V. Spagnolo, G. Scamarcio, H. Page, and C. Sirtori, Appl. Phys. Lett. **84**, 3690 (2004).
[8] M. S. Vitiello, G. Scamarcio, and V. Spagnolo, Proc. SPIE **6133**, 61330K (2006).
[9] C. Pflugl, M. Litzenberger, W. Schrenk, D. Pogany, E. Gornik, and G. Strasser, Appl. Phys. Lett. **82**, 1664 (2003).
[10] C. Pflugl (private communication).
[11] To avoid facets overheating particular care has been taken with the solder bonding to ensure uniform heat dissipation along the waveguide.
[12] J. Martinez-Pastor, A. Vinattieri, L. Carraresi, M. Colocci, Ph. Roussignol, and G. Weimann, Phys. Rev. B **47**, 10456 (1993).
[13] J. Humlicek, E. Schmidt, L. Bocanek, R. Svela, and K. Ploog, Phys. Rev. B **48**, 5241 (1993).
[14] R. Kumar, S. S. Prabhu, and A. S. Vengurlekar, Phys. Scr. **56**, 308 (1997).
[15] A. J. Shields, M. Pepper, D. A. Ritchie, M. Y. Simmons, and G. A. C. Jones, Phys. Rev. B **51**, 18049 (1995).
[16] E. X. Ping and H. X. Jiang, Phys. Rev. B **47**, 2101 (2005).
[17] The electron-lattice energy relaxation rate $(\tau_E)^{-1}$ has been calculated using the equation $\tau_E^{-1}=[N_e N k_B(R_e-R)]^{-1}$, where N_e is the number of electrons per stage, N is the number of stages, and k_B is the Boltzmann constant.
[18] It is important to note that we simultaneously extract $T_L$and $T_e$and thus R and R_e from PL measurements performed on the same laser facet point. Since the temperature does not change along the waveguide, we can assume that (R_e-R) and so τ_E^{-1} are constant along the waveguide.
[19] R. Köhler, A. Tredicucci, F. Beltram, H. E. Beere, E. H. Linfield, A. Ritchie, and A. G. Davies, Appl. Phys. Lett. **84**, 1266 (2004).
[20] G. Scalari, N. Hoyler, M. Giovannini, and J. Faist, Appl. Phys. Lett. **86**, 181101 (2005).